Author/s:
Chow, SH;Bienen, B;Randolph, M

Title:
Rapid penetration of spudcans in sand

Date:
2020

Citation:
Chow, S. H., Bienen, B. & Randolph, M. (2020). Rapid penetration of spudcans in sand. Proceedings of the 4th International Symposium on Frontiers in Offshore Geotechnics, pp.2238-2247. Deep Foundation Institute.

Persistent Link:
https://hdl.handle.net/11343/279366

RAPID PENETRATION OF SPUDCANS IN SAND

Shiao Huey Chow, Centre for Offshore Foundation Systems, The University of Western Australia, Australia, +618 6488 6930, shiaohuey.chow@uwa.edu.au
Britta Bienen, Centre for Offshore Foundation Systems, The University of Western Australia, Australia, britta.bienen@uwa.edu.au
Mark Randolph, Centre for Offshore Foundation Systems, The University of Western Australia, Australia, mark.randolph@uwa.edu.au

ABSTRACT

The growing pressure for jack-up rigs to relocate during more challenging metocean conditions for offshore wind turbine installation and maintenance has increased the risk of dynamic leg loading during the set down of the spudcan footings into the seabed. To better understand the rapid sand-spudcan interaction, this study presents experimental results of a model spudcan jacked at a range of penetration rates into dry and saturated sand at both 1*g* and 50*g* gravitational acceleration. In order to achieve a wide range of consolidation conditions, the sand was saturated using both water and a viscous pore fluid (methocel cellulose ethers) with kinematic viscosity 680 times higher than water in the 50*g* centrifuge tests. The results indicated up to 120% increase in spudcan penetration resistance due to the dilatancy-induced suction when the consolidation response changes from drained to undrained. This change in spudcan penetration resistance is quantified using a proposed backbone curve framework.

Keywords: spudcan, sand, rapid soil-structure interaction, consolidation

INTRODUCTION

Offshore renewable energy devices are typically located in shallow water with predominantly sandy seabeds. Installation and servicing of these structures, particularly wind turbines, is generally performed using mobile jack-up vessels. In ideal conditions, spudcan touch-down would occur in perfectly calm seas. In reality, there will always be some waves, and this causes motion in the jack-up, such that the spudcan touch-down may be more rapid than intended. The encountered resistance travels up the leg and must be withstood by the jack-up structure. As higher sea states result in larger forces upon spudcan touch-down, the structural integrity of the jack-up places a limiting condition on the seastate the structure can safely operate in. To define this operating envelope, the spudcan touch-down resistance must be understood accurately. The current limited ability to predict spudcan penetration resistance in sand under dynamic or rapid (undrained or partially drained) penetration conditions has introduced substantial risk. Better understanding is required of sand response under rapid shearing, particularly when this leads to generation of negative excess pore pressures that result in extremely high resistance in dilating sand as observed for other applications such as ploughing, pipelines, piezocones and plate anchors (e.g. Palmer 1999; Bransby & Ireland 2009; Chow et al. 2018, 2019).

The change in spudcan resistance with changing penetration rate (or 'rate effects') in sand can be addressed using the well-established backbone curve framework as shown in Fig. 1 (e.g. Finnie & Randolph 1994; Chow et al. 2018, 2019). The consolidation regime can be defined using a non-dimensional velocity term, $V = vd/c_v$ where v is the penetration velocity, d the spudcan diameter and c_v the coefficient of consolidation. As V increases (associated with either an increase in v and d, or a decrease in c_v), the consolidation regime will evolve from drained to partially drained to undrained conditions, with V_{dr} and V_{un} denoting the boundary between drained and undrained regime respectively in Fig. 1.

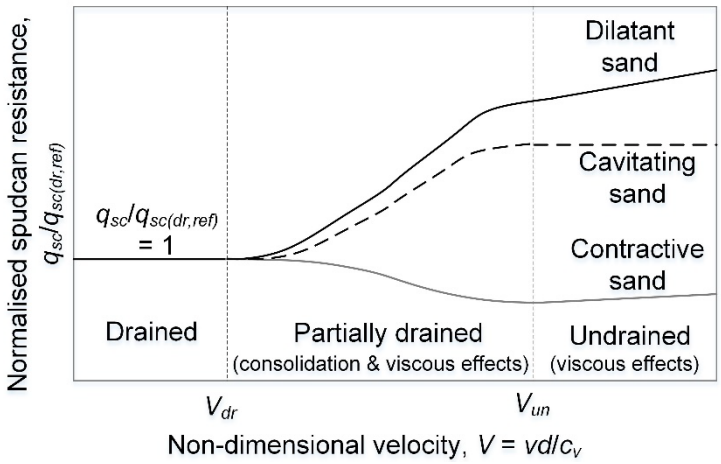

Fig. 1. Rate effects in spudcan penetration resistance in sand (modified from Chow et al. 2019)

As shown in Fig. 1, the rate effects in spudcan penetration resistance, expressed as a ratio of penetration resistance at a given penetration velocity over the drained penetration resistance at a reference velocity, $q_{sc}/q_{sc(dr,ref)}$ (where q_{sc} represents a nominal bearing resistance, force divided by the maximum spudan cross-sectional area at the shoulder) can either increase or decrease with increasing non-dimensional velocity, depending on the sand dilatancy during shearing, which is governed by the sand density, mineralogy and stress level (Bolton 1986). For contractive sands, q_{sc} will decrease with increasing V in the partially drained region ($V_{dr} < V < V_{un}$) due to positive excess pore pressure generation, while in dilatant sands q_{sc} increases with increasing V due to negative excess pore pressure generation. In principle, such positive or negative rate effects in sand are composed of two components: (a) partial consolidation effects; and (b) viscous rate effects (Lehane et al. 2009; Watanabe & Kusakabe 2013), although the latter component is likely to be relatively minor compared with the former. These effects can be captured by (Chow et al. 2019):

$$\frac{q_{sc}}{q_{sc(dr,ref)}} = \left[\frac{1+(q_{sc(un)}/q_{sc(dr,ref)})(V/V_{50})^c}{1+(V/V_{50})^c}\right]\left[\frac{1+\mu\left[(v/d)/(v/d)_{ref}\right]^n}{1+\mu}\right] \quad [1]$$

where q_{sc} is the spudcan resistance corresponding to V or v/d, $q_{sc(dr,ref)}$ the reference drained resistance at $(v/d)_{ref}$, $q_{sc(un)}$ the undrained resistance at $V = V_{un}$, V_{50} the non-dimensional velocity for 50% consolidation, v/d the penetration velocity normalised by spudcan diameter d, c a fitting coefficient that governs the curvature of the evolution of $q_{sc}/q_{sc(dr,ref)}$, μ a parameter defining the sand viscous property and n the shear-thinning index. The first term of Eq. [1] accounts for partial consolidation effects and the second term accounts for viscous rate effects using the Herschel-Bulkley formulation (Zhu & Randolph 2011). Note that viscous rate effects can also be captured using other viscous rate formulae, such as the power-law formulation (e.g. Chow et al. 2018).

For rapid penetration of spudcans in shallow waters, undrained shearing of dilating sand will lead to cavitation (e.g. McManus & Davis 1997; Palmer 1999). The occurrence of cavitation, which involves formation of vapour bubbles within the pore water, will limit the resulting spudcan penetration resistance as shown in Fig. 1. During cavitation, the sand will dilate with unrestrained volumetric change (just as in the drained response) such that the sand strength is anticipated to revert to an equivalent drained value, but with the negative pore pressure or suction limited by the absolute cavitation pressure ($u_{cav} = -p_a = -100$ kPa where p_a is the atmospheric pressure) (McManus & Davis 1997). Hence the undrained resistance upon cavitation may be computed using the existing effective stress formulation for drained penetration resistance, but adopting a confining effective stress generated by the cavitation

pressure, as discussed in Chow et al. (2019). This is explored further in the 'Test Results' section.

To examine the rate effects for spudcan penetration resistance in sand, this paper reports the findings of two experimental studies, which involved jacking a model spudcan at various penetration velocities into sand:

- Laboratory 1*g* model spudcan tests (4 tests) in dry sand (relative density, D_r = 50%) to establish viscous rate parameters (v = 0.1 to 100 mm/s or v/d = 0.0017 to 1.7)
- Centrifuge 50*g* model spudcan tests (7 tests) in saturated sand (D_r = 81 and 83%) to establish the complete backbone curve parameters ($V = vd/c_v$ = 0.6 to 33448)

TEST DETAILS

Soil Properties and Preparation

Three sand samples (one dry and two saturated) were prepared using a commercially available fine silica sand with properties listed in Table 1 (see also Chow et al. 2019). The sand samples were prepared by air pluviation into a rectangular sample container with internal dimensions of 650 mm × 390 mm × 325 mm (length × width × depth). The sand surface was vacuum levelled to produce a final sample height of 200 mm (dry) or 175 mm (saturated). The samples were saturated with either water or a viscous pore fluid (methocel cellulose ethers Grade F450 with 2.2% concentration). More details on the sample preparation and saturation using methocel is discussed in Chow et al. (2018). 60 mm layer of free fluid was maintained above the sand surface during testing.

Table 1. Properties of silica sand (Chow et al. 2019)

Specific gravity, G_s	2.67 (AS 1289.3.5.1-06)
Particle size, d_{10}, d_{50}, d_{60}	0.12, 0.18, 0.19 mm (ASTM D6913-04)
Minimum dry density, ρ_{min}	1497 kg/m^3 (ASTM D4253-00)
Maximum dry density, ρ_{max}	1774 kg/m^3 (ASTM D4254-00)
Critical state friction angle, ϕ'_{cs}	31.9° (triaxial)

A highly viscous pore fluid, methocel (Dow 2002) with kinematic viscosity $\mu_{methocel}$ ~ 680 mPas, was used in order to allow the consolidation conditions to be varied from drained to undrained, by decreasing the coefficient of consolidation, c_v (e.g. Bienen et al. 2018, Chow et al. 2018, 2019, Robinson et al. 2018). As such, the non-dimensional velocity can be increased relative to the value with water as the pore fluid (μ_{water}), according to Chow et al. (2019):

$$V = \frac{vd}{c_v}\frac{\mu_{methocel}}{\mu_{water}} \quad [2]$$

More details about the scaling consideration and modelling concept using the viscous pore fluid in centrifuge testing are provided in Chow et al. (2019).

The effective unit weights (γ') and relative densities (D_r) of the three sand samples are summarised in Table 2. The dry sample for the laboratory 1*g* tests was prepared at a relative density, D_r = 50% to ensure proper stress-dilatancy scaling taking into consideration the low stress level at 1*g*. Using Bolton's (1986) stress-dilatancy framework, the sample prepared with D_r = 50% at 1*g* is expected to produce similar relative dilatancy index ($I_R = D_r(Q - \ln p') - R$ = 4.24, where Q = 10 and R = 1) as a sample with D_r = 80% at 50*g* (Fig. 2). A similar stress scaling approach was adopted in the 1*g* model tests reported by LeBlanc et al. (2010). This will ensure the 1*g* test results can be related to the two saturated centrifuge samples prepared at a relative density, D_r = 81 and 83%, respectively.

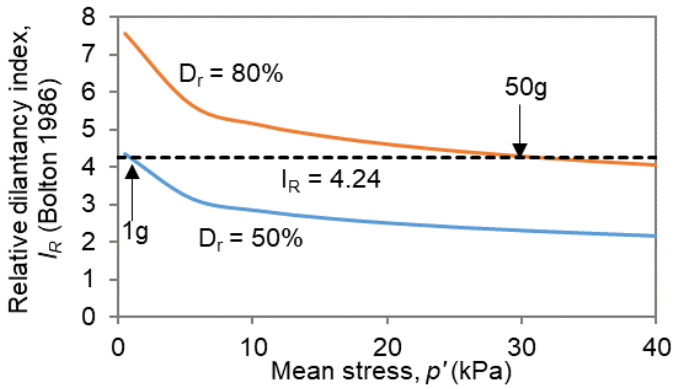

Fig. 2. Stress scaling using Bolton's (1986) framework

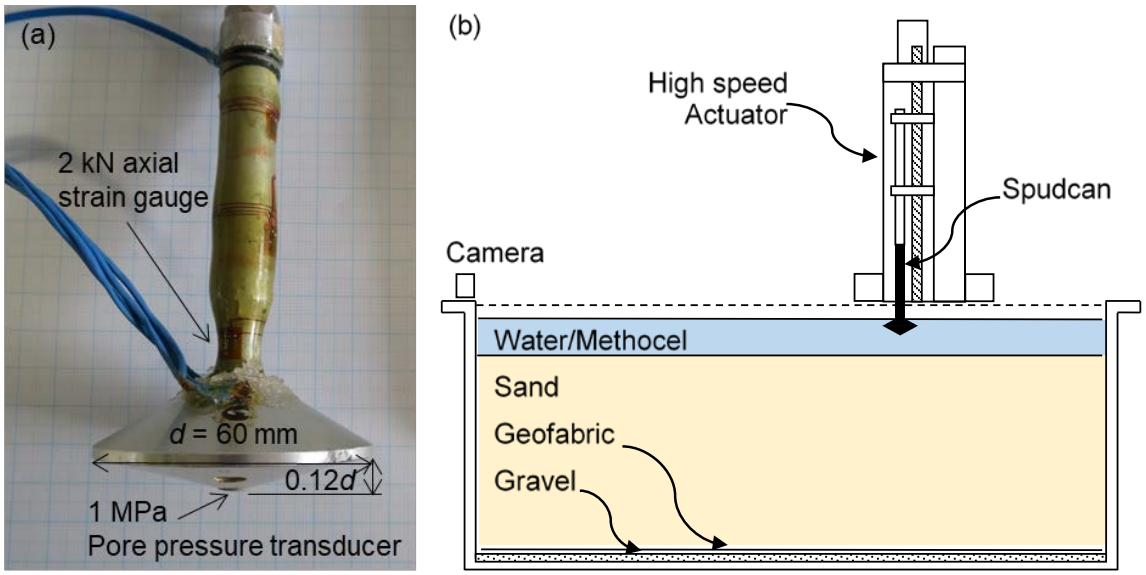

Fig. 3. (a) Model spudcan; (b) centrifuge test setup

Centrifuge test setup, procedure and programme

The model spudcan tests at 1*g* and 50*g* were conducted at the National Geotechnical Centrifuge Facility (NGCF) at the University of Western Australia. The 50*g* centrifuge tests were conducted in the 3.6 m diameter beam centrifuge with the test setup shown in Fig. 3(b). The tests involved jacking the model spudcan (Fig. 3(a)) into the sand sample at various penetration velocities using an actuator (2 kN vertical loading capacity) with maximum speed of 100 mm/s. Before each test in saturated samples, saturation checks of the pore pressure transducer filter (located at the spudcan tip) were performed by cycling the spudcan up and down in the free fluid above the soil. Satisfactory saturation was indicated by a rapid response with little or no hysteresis in the data. In addition to the axial strain gauge, the spudcan penetration resistance was also measured using an external 2 kN load cell connected to the top of loading arm. Excellent agreement was obtained between the axial strain gauge and external load cell measurements. The penetration depth of the spudcan was measured by the encoder on the motor of the vertical axis of the actuator. The model spudcan test programme is summarised in Table 2. The test can be identified as GxP, where 'G' refers to test type ('L' for laboratory 1*g* test and 'C' for centrifuge test), 'x' denotes the penetration velocity, *v* in mm/s and 'P' denotes the pore fluid ('D' for dry, 'W' for water and 'M' for methocel). For instance, Test L0.1D refers to a laboratory 1*g* test conducted at *v* = 0.1 mm/s in dry sand.

Table 2. Experimental programme

Test and sample details	Pore fluid	Test ID	$\mu_{methocel}$* (mPas)	v (mm/s)	$V = (vd/c_v)(\mu_{methocel}/\mu_{water})$
N = 1g	Dry	L0.1D	0	0.1	0
D_r = 50%		L1D	0	1	0
(γ = 15.92 kN/m^3)		L10D	0	10	0
		L100D	0	100	0
N = 50g	Water	C1W	1	1	0.6
D_r = 81%		C10W	1	10	6.1
(γ' = 10.51 kN/m^3)		C100W	1	100	61.1
N = 50g	Methocel	C1M	678	1	415
D_r = 83%		C10M	675	10	4124
(γ' = 10.55 kN/m^3)		C40M	674	40	16471**
		C80M	684	80	33448

* $\mu_{methocel}$ = 1944 $e^{-0.05T}$ determined from viscometer tests, where T = temperature in °C
** *Load cell data unreliable*

TEST RESULTS

Laboratory 1g test results: quantification of viscous rate effects

Fig. 4 presents the penetration resistance (q_{sc}) profiles to a normalised penetration depth, z/d = 1 (where z is the depth to the spudcan tip, 0.12d below the shoulder) for the 1g model spudcan tests covering v = 0.1, 1, 10 and 100 mm/s ((v/d)/(v/d)$_{ref}$ = 1, 10, 100, 1000). These tests in dry sand allow clear inspection of viscous rate (rheological) effects, as similar tests at higher v of 10 and 100 mm/s conducted in a saturated sample would have attracted both partial consolidation and viscous rate effects, evident from the measured pore pressure responses in Tests C10W and C100W (Fig. 5b). A similar strategy to isolate the partial consolidation and viscous rate effects was reported in the triaxial rate effect study in Toyoura sand described by Watanabe & Kusakabe (2013).

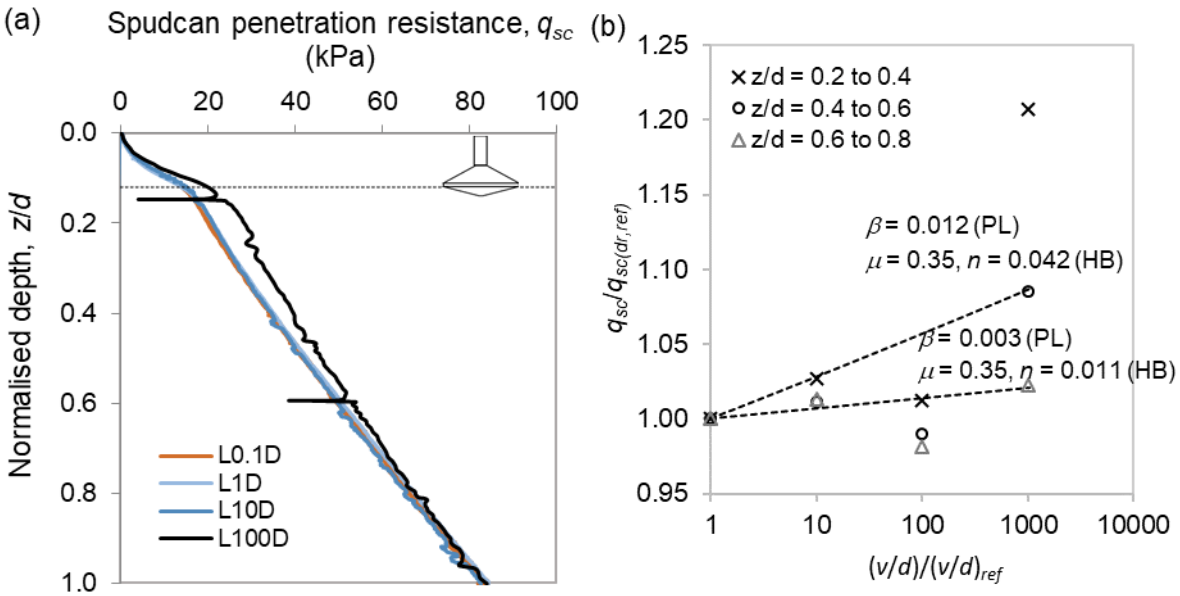

Fig. 4. 1g laboratory model spudcan test results in dry sand: (a) penetration resistance profiles; (b) quantification of viscous rate effects using Herschel-Bulkley (HB) and Power-law (PL) formulae

As shown in Fig. 4, there is negligible difference in the q_{sc} profiles between tests with the three slowest penetration velocities (v = 0.1 to 10 mm/s). However, a noticeable increase in q_{sc} is observed at the highest v = 100 mm/s. To better examine the viscous rate effect, the penetration resistance is normalised with the reference $q_{sc(dr,ref)}$ at v_{ref} = 0.1 mm/s and averaged over every z/d interval of 0.2 from z/d = 0.2 to 0.8. The range of z/d selected is to ensure the penetration resistance has achieved steady state. The averaged viscous rate effects ($q_{sc}/q_{sc(dr,ref)}$) is plotted against the normalised strain rate $(v/d)/(v/d)_{ref}$ in Fig. 4 and fitted using the Herschel-Bulkley formulation (part 2 of Eq. [1]). Fig. 4 also includes the equivalent parameters fitted using a power-law formulation ($q_{sc}/q_{sc(dr,ref)} = [(v/d)/(v/d)_{ref})]^{\beta}$) as a comparison. The fitting excludes outliers, such that $1.0 \leq q_{sc}/q_{sc(dr,ref)} \leq 1.1$. The fitted rate parameters (lower and upper bounds) for Herschel-Bulkley (μ = 0.35, n = 0.011 to 0.042) and power-law formulation (β = 0.003 to 0.012) represents 0.7 to 2.9% increase in q_{sc} per log cycle increase in normalised penetration rate, which are within the reported range of 0 to 10% increase in shear strength per log cycle increase in strain rate in sand from existing studies (e.g. Dayal & Allen 1975, Watanabe & Kusakabe 2013). A mean set of viscous rate parameters (μ = 0.35, n = 0.03) was adopted to fit the backbone curve in subsequent sections.

Centrifuge test results: establishing the backbone curve

The centrifuge spudcan test results are presented in Fig. 5. The centrifuge study involved seven spudcan penetration tests in water and methocel saturated samples, with non-dimensional velocity spanning across 5 orders of magnitude from V = 0.6 to 33448 (see test programme in Table 2). These tests allow establishment of the backbone curve encompassing the complete drained to undrained regime (Fig. 1), including quantification of the combined partial consolidation and viscous rate effects (Eq. [1]). Due to the limited vertical load capacity of the actuator, the spudcan test had to be terminated once the load cell reached 2 kN (or q_{sc} = 700 kPa) to avoid equipment failure. This resulted in very shallow spudcan embedment of $z/d \leq 0.18$.

As shown in Fig. 5a, the spudcan penetration resistance or nominal bearing pressure (q_{sc}) increases between 50% and 120% (depending on z/d) as V increases from 0.6 to 33448. The increase in q_{sc} is caused by a corresponding decrease in the pore pressure (suction) at the tip, due to the sand dilation (Fig. 5b). The pore pressure profiles indicate that the slowest test at V = 0.6 produces drained response, while tests with $V \geq 6$ produce partially drained response with generation of suction. It is interesting to observe that positive excess pore pressure was measured initially for $z/d \leq 0.02$ before generation of suction at deeper depths. The maximum positive pore pressure of 220 kPa, at z/d = 0.02 should be seen in the context of the true average bearing stress at that depth (as the plotted nominal bearing pressure q_{sc} ~ 30 kPa is computed using the full area instead of the partially embedded cross-sectional area), which will be $(0.12/0.02)^2$ or 36 times higher (so just over 1000 kPa). Hence the positive pore pressure still suggests dilation is occurring, since the pore pressure is so much less than the applied total stress, assuming essentially undrained conditions for the highest penetration rate.

The measured spudcan resistance and pore pressure are observed to reach a plateau for $V \geq 4124$ for penetrations exceeding $0.08d$. The limiting q_{sc} and u at $V \geq 4124$ suggests the presence of undrained spudcan resistance associated with cavitation, as was also reported for undrained triaxial tests and suction caisson uplift tests (e.g. McManus & Davis 1997; Byrne & Houlsby 2002). However, the measured limiting u_{cav} ~ -30 kPa (beyond z/d > 0.08) is only one-third of the expected cavitation pressure u_{cav} = -100 kPa (Fig. 5b). The limiting u_{cav} of around -30 kPa is likely to be caused by the point measurement right under the conical tip, where there is a complex distribution of normal stress induced pore pressure (positive) and shear stress induced pore pressure (negative) as shown by the numerical study of spudcan undrained capacity in silty clay (Ragni et al. 2017) and also discussed in cone penetrometer

studies in dilating soil (e.g. Burns & Mayne 2002). Inevitably, local concentrations of the excess pore pressure field will lead to initiation of cavitation away from the pore pressure measurement location, so that the measured u_{cav} does not reach the theoretical limit.

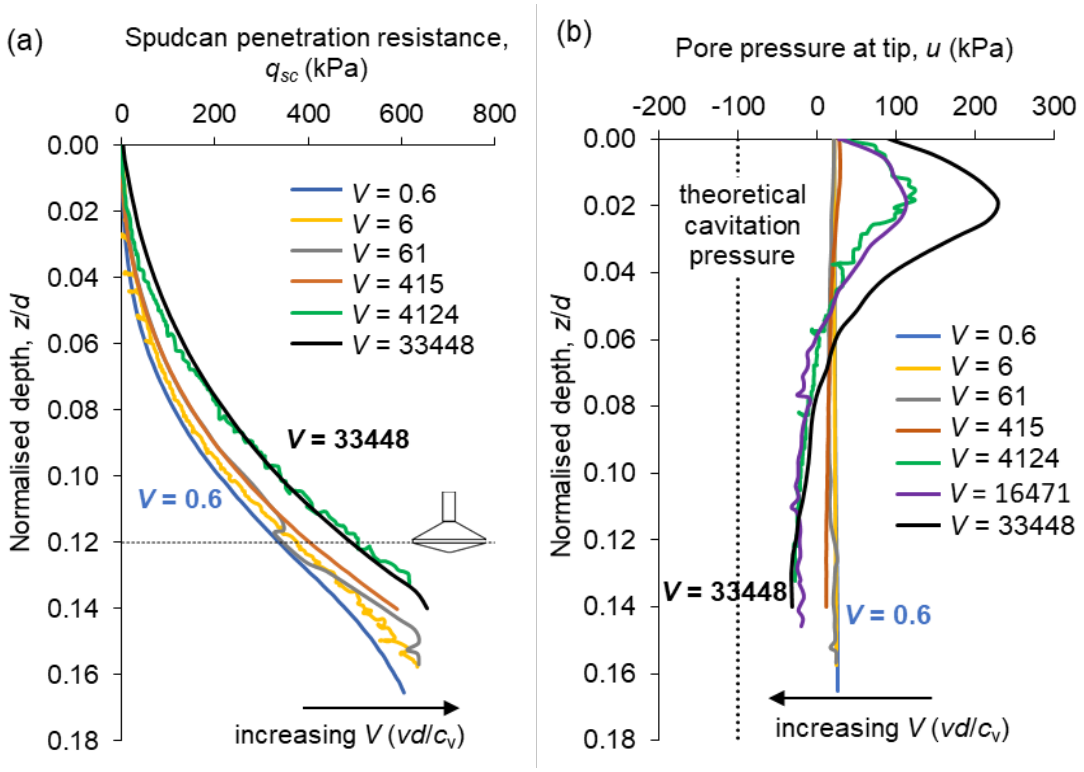

Fig. 5. Centrifuge spudcan test results: (a) penetration resistance; (b) pore pressure profiles

Fitting of the backbone curve

To examine the combined rate effects using the backbone curve expressed by Eq. [1], the normalised penetration resistance, $q_{sc}/q_{sc(dr,ref)}$ (where V_{ref} = 0.6) are computed and averaged over every z/d interval of 0.02 from z/d = 0.06 to 0.12. The range of z/d selected is to ensure the penetration resistance has achieved a steady state. The averaged normalised resistance ($q_{sc}/q_{sc(dr,ref)}$) is plotted against the non-dimensional velocity, $V=(vd/c_v)(\mu_{methocel}/\mu_{water})$ computed using c_v = 9.81 x 10^{-5} m^2/s at σ'_v =13 kPa and D_r = 83% (determined from Rowe cell tests) in Fig. 6a. The backbone curve in Fig. 6a shows that the transition from drained to partially drained conditions occurs at V_{dr} = 6, and the transition from partially drained to undrained conditions at V_{un} = 4000 respectively. Using the mean viscous rate parameters determined from the 1*g* tests (μ = 0.35, n = 0.03), the experimental data in Fig. 6a is fitted using Eq. [1] to obtain the partial consolidation rate parameters of $q_{sc(un)}/q_{sc(dr,ref)}$ = 2, V_{50} = 175 and c = 0.8 as summarised in Table 3. The respective contribution of the partial consolidation and viscous rate effects are also plotted in Fig. 6a.

Table 3 also includes the fitted backbone curve parameters reported for piezocone and rectangular plate anchor tests in the same sand (Chow et al. 2018, 2019). As these applications involve different object geometry and size, strain rate (v/d) and loading mechanism, a consolidation index (CI) modified from Lee & Randolph (2011) is used here to compare the rate effects in the three different applications:

$$CI = \frac{q_{sc}/q_{sc(dr,ref)} - 1}{q_{sc(un)}/q_{sc(dr,ref)} - 1} = \frac{(V/V_{50})^c}{1+(V/V_{50})^c} \quad [3]$$

where *CI* of 0 and 1 correspond to the limits of fully drained and fully undrained conditions, respectively. The *CI* curves for the spudcan, piezocone and plate anchors are presented in Fig. 6(b). The spudcan and plate anchor are found to produce similar *CI* curves, albeit differing through a steeper curvature (*c*) and narrower range of V_{dr} and V_{un} for the plate anchor. Due to the much shorter drainage path for the piezocone (d = 0.01 m), the *CI* curve of the piezocone shifts towards the right of the other two applications with larger (equivalent) diameter ($d_{spudcan}$ = 0.06 m and $d_{plate\ anchor}$ = 0.032 m).

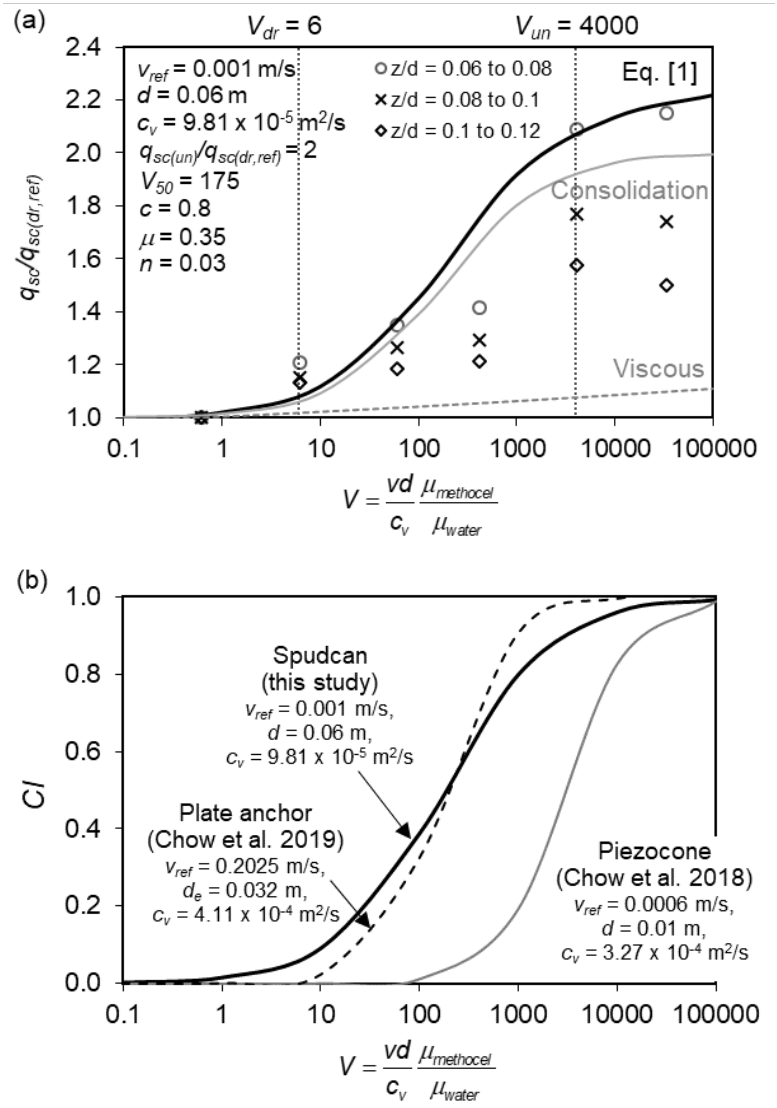

Fig. 6. Fitting of backbone curve parameters: (a) individual contribution of partial consolidation and viscous rate effects; (b) comparison with other studies in the same sand

Table 3. Best-fitted parameters for backbone curves

Application	d or d_e (m)	v_{ref} (m/s)	c_v (m^2/s)	D_r (%)	V_{dr}	V_{un}	$q_{(un)}/q_{(dr,ref)}$	V_{50}	c	β	μ	n
Spudcan	0.06	0.001	9.81 x 10^{-5}	83	6	4000	2	175	0.8	0.008	0.35	0.03
Piezocone[1]	0.01	0.0006	3.27 x 10^{-4}	83	7	-	4	3000	1.3	0.023	0.35	0.075
Plate anchor[2]	0.032	0.2025	4.11 x 10^{-4}	82	16	540	2.2	175	1.3	0.016	0.35	0.05

[1] *Chow et al. (2018)*
[2] *Chow et al. (2019)*

SUMMARY AND CONCLUSIONS

This study has investigated rate effects in spudcan penetration resistance in sand encompassing fully drained to fully undrained regime, allowing capturing of a backbone curve relating normalised bearing resistance to normalised penetration rate. Through isolation of the separate rate effect components reflecting degree of consolidation and viscous shearing, the study has confirmed that viscous rate effects are secondary to partial consolidation effects in sand. The spudcan resistance is found to increase up to 120% when evolving from drained to undrained conditions in dense sand, reflecting the range of soil (and spudcan) conditions found in areas of offshore wind farm development. The significant increase in spudcan resistance under partially drained and undrained conditions results from dilation induced negative pore pressures, although the undrained resistance is limited by occurrence of cavitation due to the low total stress. The measured cavitation pressure (u_{cav} = -30 kPa) does not reach the theoretical value of -100 kPa, as has been found in other studies, attributable to initiation of cavitation at local concentrations of suction, rather than at the measuring point. The complex pore pressure response during rapid penetration of spudcan requires further study, which is currently ongoing using large deformation dynamic coupled analysis with allowance for cavitation; suitable constitutive models are implemented with the ability to capture the stress-dilatancy of sand accurately. For application in practice, the backbone curve for the spudcan can be established using cone penetrometer tests through correlation using the consolidation index, *CI* (Eq. [3]), taking into consideration the difference in size and geometry between the spudcan and penetrometer and introducing appropriate time and size scaling to achieve compatible consolidation conditions. The penetrometer-based design method will be developed following synthesis of ongoing experimental and numerical studies.

ACKNOWLEDGEMENTS

This work forms part of the activities of the Centre for Offshore Foundation Systems (COFS), currently supported as a Centre of Excellence by the Lloyd's Register Foundation. The Lloyd's Register Foundation invests in science, engineering and technology for public benefit, worldwide. The work is also supported by the Australian Research Council Discovery Grant Scheme DP190100914.

REFERENCES

Australian Standard, 2006. AS 1289.3.5.1-06 Soil classification tests – determination of the soil particle density of a soil – Standard method. Standards Australia.

ASTM, 2009. ASTM D6913-04 (2009) Standard test method for particle-size distribution (gradation) of soils using sieve analysis. American Society for Testing and Materials, West Conshohocken, Pennsylvania, USA.

ASTM, 2006. ASTM D4253-00 (2006) Standard test method for maximum index density and unit weight of soils using a vibratory table. American Society for Testing and Materials, West Conshohocken, Pennsylvania, USA.

ASTM, 2006. ASTM D4254-00 (2006) Standard test method for minimum index density and unit weight of soils and calculation of relative density. American Society for Testing and Materials, West Conshohocken, Pennsylvania, USA.

Bienen, B., Klinkvort, R.T., O'Loughlin, C.D., Zhu, F. and Byrne, B.W. 2018. Suction Caissons in Dense Sand, Part I: Installation, Limiting Capacity and Drainage. Géotechnique (11):1–47.

Bolton, M.D. 1986. The strength and dilatancy of sands. Géotechnique 36(1): 65–78.

Bransby, M.F. and Ireland, J. 2009. Rate effects during pipeline upheaval buckling in sand. ICE Geotechnical Engineering 162(5): 247–256.

Burns, S.E. and Mayne, P.W. 2002. Analytical cavity expansion-critical state model for piezocone dissipation in fine-grained soils, Soils and Foundations 42(2): 131–137.

Byrne, B.W. and Houlsby, G.T. 2002. Experimental investigations of response of suction caissons to transient vertical loading. Journal of Geotechnical & Geoenvironmental Engineering 128(11): 926–939.

Chow, S.H., Bienen, B. and Randolph, M.F. 2018. Rapid penetration of piezocones in sand. Proceedings of the 4th International Symposium on Cone Penetration Testing (CPT'18), Delft, pp. 213-219.

Chow, S.H., Diambra, A., O'Loughlin, C.D., Gaudin, C. and Randolph, M.F. 2019. Consolidation effects on monotonic and cyclic capacity of plate anchors in sand. Géotechnique. https://doi.org/10.1680/jgeot.19.ti.017.

Chow, S.H., Roy, A., Herduin, M., Heins, E., King, L. Bienen, B., O'Loughlin, C.D., Gaudin, C. and Cassidy, M.J. 2019. Characterisation of UWA superfine silica sand. Oceans Graduate School Technical Report, The University of Western Australia, Geo 18844. https://doi.org/10.26182/5d8c185bcd366.

Dow, 2002. Methocel Cellulose Ethers: Technical Handbook. The Dow Chemical Company, Staines, UK.

Finnie, I.M.S. and Randolph, M.F. 1994. Punch-through and liquefaction induced failure of shallow foundations on calcareous sediments. Proceedings of the International Conference on Behaviour of Offshore Structures. Boston, MA, 217 – 230.

Leblanc, C., Houlsby, G.T. and Byrne, B.W. 2010. Response of stiff piles in sand to long-term cyclic lateral loading, Géotechnique 60(2): 79–90.

Lee, J. and Randolph, M.F. 2011. Penetrometer-Based Assessment of Spudcan Penetration Resistance, Journal of Geotechnical and Geoenvironmental Engineering 137(6): 587–596.

Lehane, B.M., O'Loughlin, C.D., Gaudin, C., and Randolph, M.F. 2009. Rate effects on penetrometer resistance in kaolin. Geotechnique 59(1): 41–52.

McManus, K.J. and Davis, R.O. 1997. Dilation-induced pore fluid cavitation in sands. Géotechnique 47(1): 173-177.

Palmer, A.C. 1999. Speed effects in cutting and ploughing. Géotechnique 49(3): 285–294.

Ragni, R., Bienen, B., Wang, D., Mašín, D. and Cassidy, M.J. 2017. Numerical modelling of the effects of consolidation on the undrained spudcan capacity under combined loading in silty clay. Computers and Geotechnics 86: 33–51.

Robinson, S., Brown, M.J., Matsui, H., Brennan, A., Augarde, C.E., Coombs, W. and Cortis, M. 2018. Centrifuge testing to verify scaling of offshore pipeline ploughs. International Journal of Physical Modelling in Geotechnics 19(6): 305-317.

Watanabe, K. and Kusakabe, O. 2013. Reappraisal of loading rate effects on sand behavior in view of seismic design for pile foundation. Soils and Foundations 53(2): 215-231.

Zhang, Z., Bienen, B. and Cassidy, M.J. 2013. Development of a combined VHM loading apparatus for a geotechnical drum centrifuge, International Journal of Physical Modelling in Geotechnics 13(1): 13–30.

Zhu, H. and Randolph, M.F. 2011. Numerical analysis of a cylinder moving through rate-dependent undrained soil. Ocean Engineering 38(7): 943–953.